SNO-STR-97-034

IMPLEMENTATION OF A SUPERNOVA GENERATOR CODE FOR THE SUDBURY NEUTRINO OBSERVATORY MONTE CARLO ANALYSIS SOFTWARE

By

Hui-Siong Ng

A THESIS SUBMITTED IN PARTIAL FULFILLMENT OF
THE REQUIREMENTS FOR THE DEGREE OF
BACHELOR OF SCIENCE

in

THE FACULTY OF SCIENCE
DEPARTMENT OF PHYSICS AND ASTRONOMY

We accept this thesis as conforming
to the required standard

.....

.....

THE UNIVERSITY OF BRITISH COLUMBIA

April 1997

Abstract

The Sudbury Neutrino Observatory (SNO), though built for solar neutrino detection, is also sensitive to supernova neutrinos. The use of heavy water (D_2O) as the interacting medium provides sensitivity to all species of neutrinos. This gives SNO a rather unique opportunity in the study of new physics parameters, particularly the neutrino mass. The purpose of this work is to simulate supernova neutrino signals in SNO. This required the writing of a supernova generating code whose supernova model is based on that of Burrows and Klein.

From the simulation, SNO is expected to detect about 783 ± 24 events for a 10 kpc supernova. Further distances like SN1987A will give 33 ± 6 events. The average energies of the neutrinos are 16.5 ± 1.5 MeV, 18.2 ± 0.9 MeV, and 26.0 ± 1.8 MeV for ν_e , $\bar{\nu}_e$, and ν_μ respectively. The directional resolution of the detector is found to be around $4.0° \pm 0.7°$ for a 10 kpc supernova. However, this resolution degrades rapidly for more distant supernova.

Testing of the generator code has yielded results that agree with the published work of Burrows. Linking with the SNO analysis software, SNOMAN, has been successful. SNOMAN can now reproduce the input angular and energy distribution of supernova neutrinos. The only remaining problem is SNOMAN's inability to reproduce the time distribution. This may be attributed to a problem within SNOMAN's time storage bank, which will be fixed by the SNOMAN authors.

Table of Contents

Abstract ii

Table of Contents iii

List of Tables v

List of Figures vi

Acknowledgements vii

1 Introduction 1

1.1 Supernova Mechanism 2

1.2 Neutrino Signal of Stellar Collapse 4

1.2.1 The early phase: Infall and Flash 4

1.2.2 The middle phase: Accretion and Explosion 6

1.2.3 The late phase: Protoneutron star cooling 6

1.3 Supernova Detector 7

2 The SNO Detector 9

2.1 Neutrino Interactions 11

3 Supernova Generator 13

3.1 SNO Monte Carlo Analysis Software 13

3.2 Motivation 14

3.3 SN Generator Code 15

4 Signal Formalism 18

4.1 Neutrino Emission Model 18

4.2 Sampling and Detection 19

5 Results **22**

5.1 Event Distribution 22

5.1.1 Count Rate 23

5.1.2 Expected Events 26

5.1.3 Energy Distribution 26

5.2 SNOMAN's Output 27

5.3 Simulation of SN1987A 30

5.4 Future Implementations 33

6 Conclusions **35**

A Rejection Method **37**

B Coordinate Transformation **39**

Bibliography **41**

List of Tables

2.1 The ν interactions in SNO detector and their Q values 12

3.1 Input Parameters for the Neutrino Interactions in SNO 16

5.1 Expected number of events for SNO using different supernova models . . 27

List of Figures

1.1 The different stages of a Type II supernova 3
1.2 Luminosity curve of neutrino emission for a Type II supernova 5

2.1 Diagram of the SNO detector 10

5.1 Event distribution of ν_e , $\bar{\nu}_e$, and ν_μ for a 10 kpc supernova as seen by the SNO detector 24
5.2 Count rate of the SNO detector for a 10 kpc supernova 25
5.3 Energy distribution for ν_e , $\bar{\nu}_e$, and ν_μ obtained by sampling the normalized detected neutrino flux distribution 28
5.4 Comparison between sampled and SNOMAN's output energy distribution for $\bar{\nu}_e + p$ 28
5.5 Time distribution output by SNOMAN 29
5.6 Fitted direction cosine distribution output for $\bar{\nu}_e + p$ 31
5.7 Fitted direction cosine distribution output for ES interaction 32
5.8 Event Distribution of SNO for a 50 kpc supernova 33
5.9 Energy distribution comparison between observed and simulated $\bar{\nu}_e$ events for a 50 kpc supernova 34

A.1 Schematic on performing rejection method for sampling the distribution $p(x)$ 38

B.1 Schematic diagram for the derivation of the direction cosines 40

Acknowledgements

I am especially grateful for the support and help of my supervisor, Prof. Chris Waltham. He has been very helpful in pointing out the subtle things one needs to consider when doing this kind of simulation. Also he has been very patient despite the slow progress of my work. He has been most helpful in providing me with all the guidance for doing the calculations. I would like to thank Rob Komar, Christian Nally and Alan Poon for helping me decrypt the SNO simulation program, SNOMAN. Thanks go to Richard Helmer of TRIUMF for the suggestion on this topic. Thanks also go to Joshua Klein of University of Pennyslavania for getting me started on the generator code and Jaret Heise for the encouragement.

Chapter 1

Introduction

He saw; and blasted with excess of light. Closed his eyes in endless night,

–Thomas Gray (1716-1771)
The Progress of Poesy

At approximately UT 7:35:35, 23 February 1987, the first signal of the blue supergiant star, Sanduleak -69° 202 in the Large Magellanic Cloud, undergoing core collapse and exploded 100000 years ago arrived on Earth. The neutrinos from the supernova left their marks in two water Cerenkov detectors designed for proton decay detection, Kamiokande II in Japan and IMB in US, one hour before the spectacular celestial firework display in optical wavelengths. A sparse total of 20 neutrinos were observed for both detectors; however the significance of these events cannot be understated. For the first time in modern science history, mankind is able to probe the inaccessible region of the dense supernova core. These 20 events have provided a direct experimental confirmation of the stellar collapse model. They have also placed a new lower limit on the mass of $\bar{\nu}_e$ of $\leq$ 20 eV, and in doing so, tested the weak interaction on the extragalactic length scale.

These few events have also left many unanswered questions on the precise mechanism that leads to a supernova explosion and opened up the possibility of detecting new physics parameters using supernova neutrinos. These questions will be addressed by the next generation of neutrino detectors, if Nature provides another galactic supernova during the operational period of these detectors. This chapter contains the general description of the mechanism of stellar collapse and also the description of a new neutrino detector, the Sudbury Neutrino Observatory.

1.1 Supernova Mechanism

Stellar evolution is a constant battle between pressure and gravity. Ignition of a thermonuclear fuel temporarily halts the gravitational collapse of the star. However, as each fuel is exhausted, the stellar core contracts and hence increases its temperature. In this way, the stellar core evolves through successive stages of increased temperature, density and atomic weights, producing a structure of nested shells of light elements. For massive stars ($\geq 8M_{\odot}$), continued thermonuclear burning of heavier elements gives rise to iron cores which eventually will reach the Chandrasekhar mass of 1.4 $M_{\odot}$, the lower mass limit for core collapse. The first stage of collapse occurs when the pressure of the electron gas of the core is unable to support the inward pressing gravitational pressure. The core loses pressure support and implodes homologously. As the collapse proceeds, the flow breaks up into a subsonic inner core and a supersonic outer core. Once the subsonic core attains nuclear densities, the forces between the nonrelativistic nucleons are able to provide the pressure necessary to halt any further collapse. This stiffening of the inner core causes the inner core material to rebound into the supersonic outer core, creating a shockwave at the interface between them.

Travelling at a speed near $c/3$, the shockwave dissociates the outer mantle as it works its way out in mass and radius, possibly becoming the supernova explosion itself. This direct formation of a supernova is known as the prompt mechanism. However, calculations have shown that the shock will fizzle into a accretion shock instead of a supernova around 43 msec after bounce, making the prompt mechanism somewhat doubtful. Another mechanism that has been proposed involves a reheating of the accretion shock by the neutrinos from the core over periods of a hundred millseconds which will eventually revive the shock into a supernova. This delayed mechanism, as it is called, is favored over the prompt mechanism since the core is found to ring after the shock [1]. Perhaps a proper model for this phase could be developed if physicists could perform the correct 3-D hydrodynamic convection calculations. After the explosion, the hot dense core of the protoneutron star will cool off by emitting neutrinos. Much of the information about the supernova has already been carried away by the weakly interacting neutrinos before any photons are emitted from the supernova. The different stages of the supernova is summarized in Fig. 1.1. The early arrival of these neutrinos presents a potential early supernova

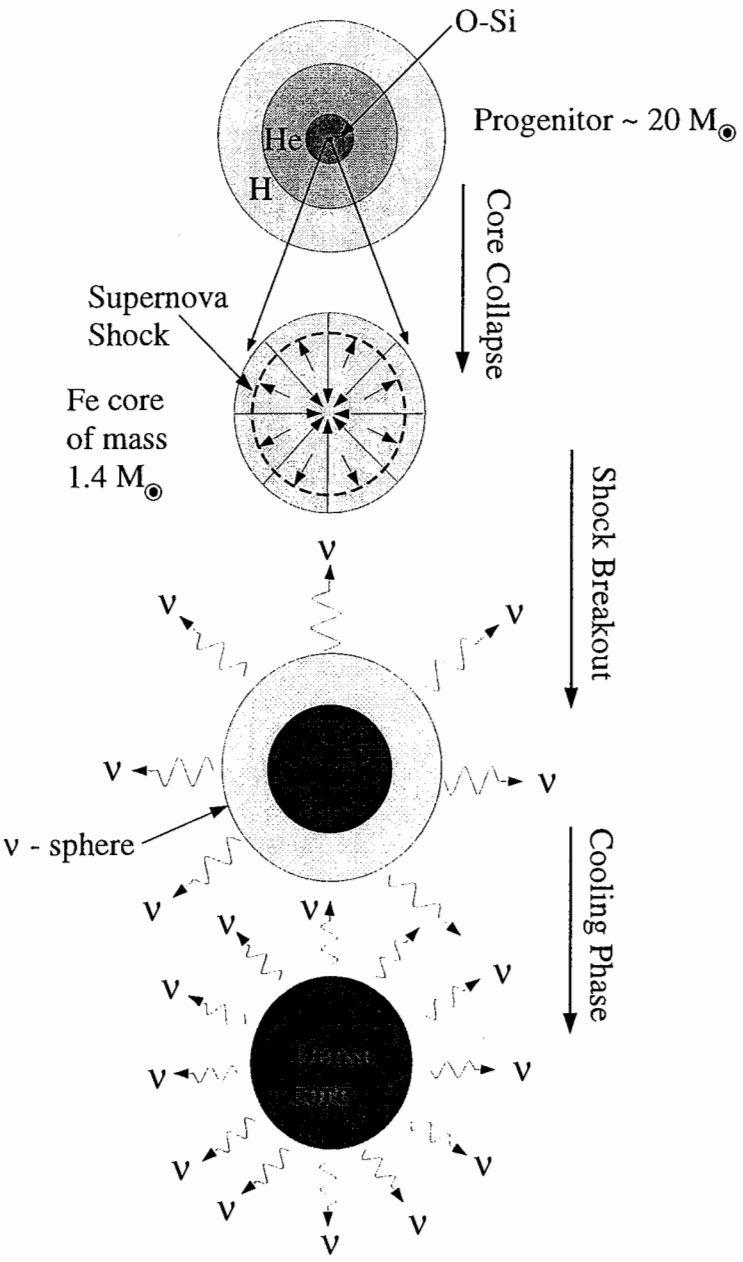

Figure 1.1: Diagram showing the different stages of a Type II supernova (not to scale). The mass of the progenitor is about 20 $M_{\odot}$. Layers of light elements are found further out from the iron core where nuclear fusion cannot proceed any more. Shown is the 1.4 $M_{\odot}$ iron core undergoing core collapse.

warning system for astronomers working in the electromagnetic spectrum. The spectrum of the neutrinos emitted during the different stages of the collapse are discussed in the following section.

1.2 Neutrino Signal of Stellar Collapse

1.2.1 The early phase: Infall and Flash

During the infall stage, the electron neutrino luminosity increases dramatically due to electron capture on the nuclei and the superallowed electron capture process by protons:

$$e^- + p \rightarrow n + \nu_e \tag{1.1}$$

The electron neutrino spectra during the infall stage is nonthermal and of a capture type spectrum. The capture spectrum can be quite complicated since it entails electron capture on free protons and nuclei. However, it is still possible to model the spectrum using a thermal spectrum with temperature of 1.7 MeV and degeneracy parameter $\eta_{\nu_e} = 11.0$ [2]. As mentioned earlier, the infall stage does not continue indefinitely but will stop when the core reaches nuclear densities and create a bounce. The shockwave formed in the bounce will transverse the *neutrinospheres* for all the species of neutrinos located at 50 to 100 km from the center in about 2 msec. The neutrinosphere is defined to be the radius of the sphere where the opacity for the neutrinos is unity. The shock will deposit some of its energy to the ν_e trapped within the neutrinosphere, enabling them to escape from the neutrinosphere, thus creating a ν_e flash, causing the peak in Fig. 1.2. This is the first burst signal that one would be able to detect. The energy deposited by the shock will cause the rapid turn-on of the $\bar{\nu_e}$ and ν_μ emission[1]. At this point, the main neutrino creation process is pair annihilation of electron and positron pairs [3]:

$$e^+ + e^- \rightarrow \nu_x + \bar{\nu_x}, \quad x = \mathrm{e}, \mu, \tau \tag{1.2}$$

The $\bar{\nu_e}$ and ν_μ that are trapped will gradually emerge from the core around 20 msec after bounce as heat from the shocked mantle reaches the neutrinosphere. After shock

[1] ν_μ is all other types of neutrinos beside from ν_e and $\bar{\nu_e}$

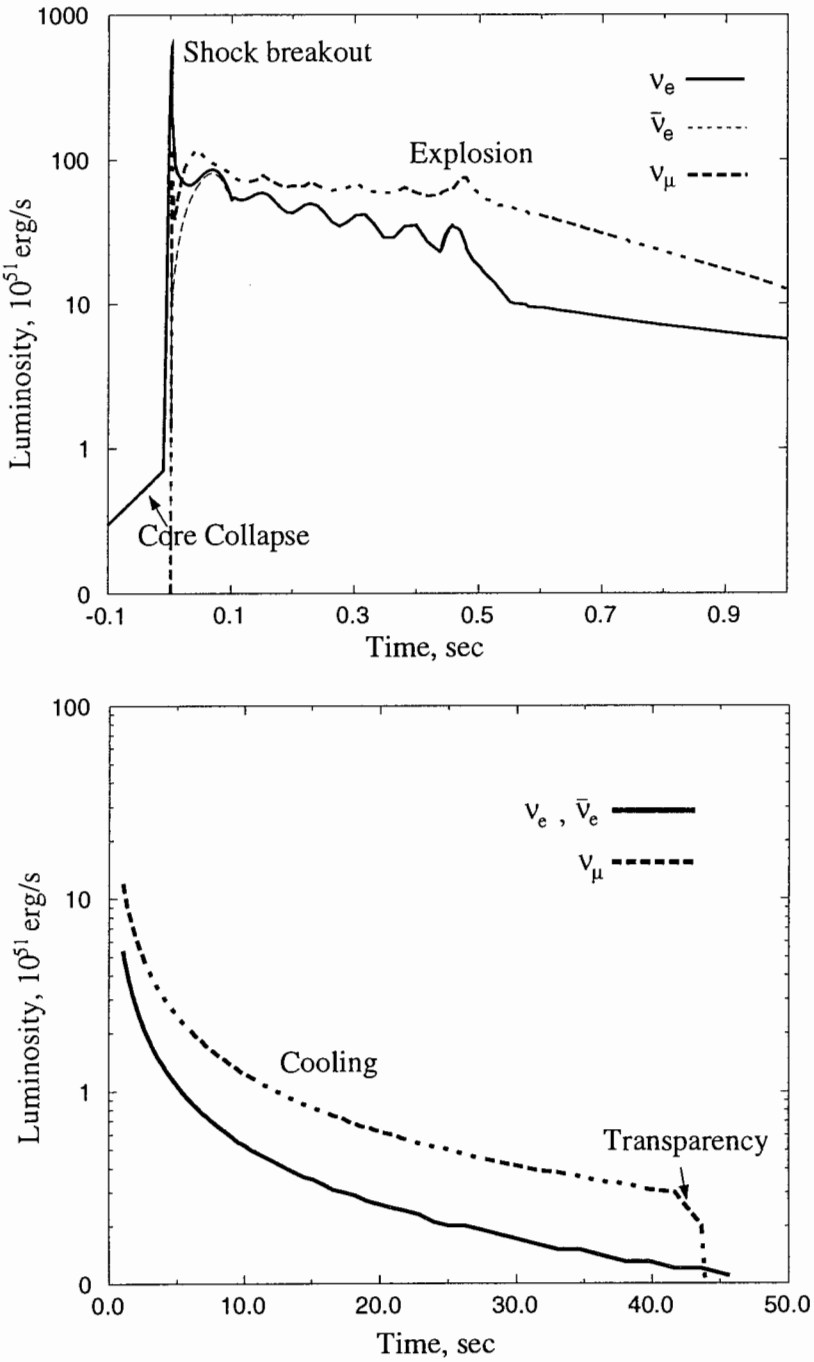

Figure 1.2: Luminosity curve for all species of neutrinos for a Type II supernova. The oscillatory part is due to the delayed mechanism where the core rings. After 0.1 sec, the luminosity of $\bar{\nu_e}$ is identical to that of ν_e .

breakup, the ν_e spectrum will make a radical transition to a thermal distribution with energy around 10 MeV.

1.2.2 The middle phase: Accretion and Explosion

The neutrino emission used assumes a delayed mechanism that leads to the eventual explosion of the supernova. In this case, the neutrinos luminosities will oscillate at a period of 80 msec until the accretion shock is re-energized and induces the supernova explosion. At explosion, the luminosities for all neutrinos will increase for a short period of time.

1.2.3 The late phase: Protoneutron star cooling

After the supernova explosion, the protoneutron star will cool by the emission of neutrinos. Even though the supernova is luminous in the first few hundred milliseconds, most of the emitted energy comes from the cooling of the protoneutron star. The cooling occurs at two stages: the middle accretion/mantle cooling phase and the long-term cooling phase. The former phase cools off with a decay constant of 1 sec while that of the latter is around 4 sec. The neutrino luminosity decays as a power law (index $\sim 1 \pm 0.5$) due to the nonlinear nature of neutrino transport. The long duration of the late cooling phase is due to the high densities of the protoneutron star and the high energies of the neutrinos leading to a higher opacities. At this stage, the neutrino spectra can be described by a Fermi-Dirac distribution with temperature T_{ν_e}=4.0 MeV for ν_e and $\bar{\nu}_e$ while ν_μ will be at 7.0 MeV. The cooling phase will terminate rapidly once the core becomes transparent. At this point, neutrino trapping ceases and the creation of neutrinos through process (1.2) will stop. This occurs at $t = 46$ and 42 sec for ν_e ($\bar{\nu}_e$) and ν_μ respectively [2]. The luminosities of the neutrino will plummet rapidly due to the lack of neutrino supply within the core. An observed abrupt turnoff in the neutrino luminosity 1 sec after the explosion will reveal the birth of a black hole instead of a neutron star.

1.3 Supernova Detector

In order to extract as much information about the supernova as possible, it is highly desirable to have a neutrino detector with a high detection rate to provide statistical viable data. The event rate is dictated by the numbers of particles in the detector volume and the cross-section for the interaction (the higher the better). Thus a high event rate can be achieved by increasing the volume of the detector; the new detector SuperKamiokande (50000 kton water) is a fine example. SNO, though relatively small in volume (1 kton), employs heavy water which has a higher interaction cross-section, making the number of detected neutrinos comparable to SuperKamiokande.

Light water detectors are only sensitive to ν_e and $\bar{\nu_e}$ and hence a definitive determination of the total neutrino flux cannot be done using these detectors. On the other hand, the deuterons used by SNO can interact with all species of neutrinos (see Sec. 2.1) and thus are able to determine the total neutrino flux from a supernova. Event identification is somewhat difficult using a light water detector since detection is based on the Cerenkov photons emitted by the electrons or positrons. Event identification will not pose much of a problem for SNO since it is possible to correlate the Cerenkov light with the neutron detection.

In any neutrino detector, a low background is crucial to the sensitivity of the detector. This is particularly important for solar neutrino detection due to the lower neutrino energy. For supernova neutrino detection, the main backgrond would be high energy muon events from cosmic rays which will not be a factor for SNO due to its depth (2 km). Presently SNO has the lowest background of all neutrinos detectors due to its depth and measures taken to ensure minimal radioactivity during construction.

Typical supernova events will consist of a burst within 20 ms, followed by a steady event rate over tens of seconds. The detection system must be able to resolve the high event rate, must have buffers to store the events and an accurate clock to determine the time of each event. The overall SNO timing resolution is on the microsecond scale while the memory can handle 4 MHz event rate. The SNO timing system consists of two separate high precision oscillators. With the existing electronics and detecting system, SNO will be able to resolve any supernova within the galactic neighbourhood. It can be concluded that SNO, though built for solar neutrino detection, is undoubtedly an

excellent supernova detector. Supernova neutrino detection will be a bonus to the project. The low count rate and energy of solar neutrinos will not interfere with the detection.

Chapter 2

The SNO Detector

The Sudbury Neutrino Observatory (SNO), located 2 km underground in the Creighton mine near Sudbury, Ontario, will be a 1.0 kton heavy water detector when construction is completed in late 1997. The heavy water will be enclosed in a 12 m diameter acrylic vessel which will be surrounded by 1.6 kton of ultrapure light water which acts both as an interacting medium and background shielding. Background from cosmic rays and detector materials is reduced by: (i) the depth of the detector underground, (ii) extreme low radioactive content in the construction material, and (iii) shielding provided by the light water and the urylon lining on the cavity wall. A diagram of the detector can be found in Fig. 2.1. Heavy water has the distinct advantage of being able to detect all species of neutrinos through neutral current interactions as well as charged current interactions.

The detection of Cerenkov light from neutrino interactions will be done by the 10000 Hamamatsu R1408 photomultiplier tubes (PMTs). These PMTs will provide about 65% photocoverage of the detector giving an overall efficiency of 90% for the high energy neutrinos from a supernova. The typical response time of a PMT is about 10 ns. Events which produce neutrons will be detected through: (i) neutron capture on water, emitting a γ ray or (ii) ^{3}He proportional counters immersed in the heavy water. Another method of enhancing the number of neutron capture is to add additives ($MgCl_2$ salt) into the heavy water which will improve the detectability of the neutrons from the neutral current events.

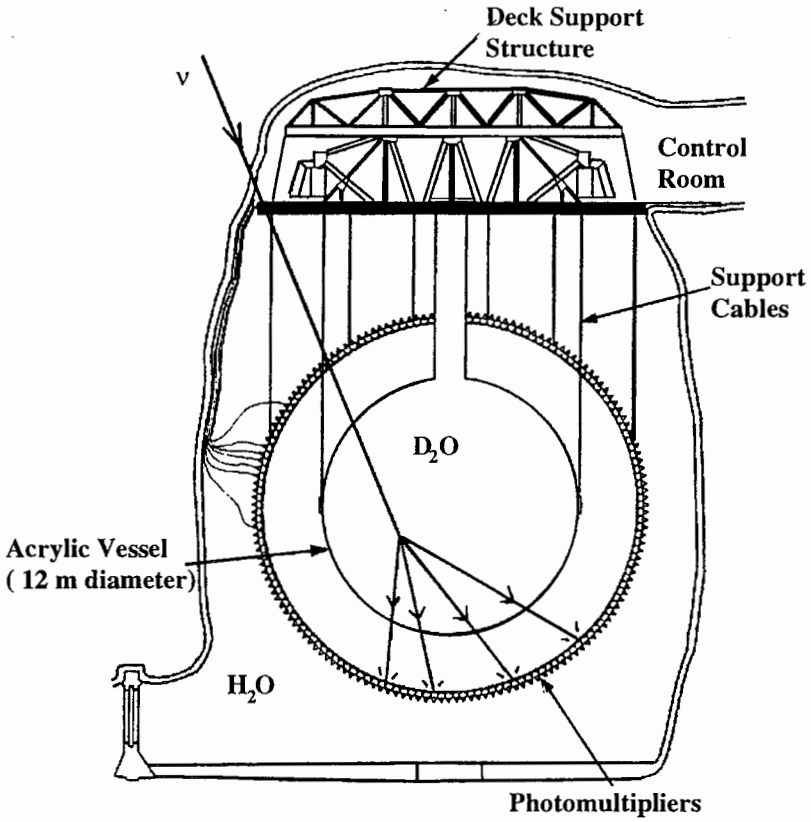

Figure 2.1: Diagram of the SNO detector. The acrylic vessel is surrounded by ten thousand PMTs giving a photocoverage of about 65%. The detector cavity will be filled with ultrapure light water while the vessel will be filled with heavy water. The cavity wall has a urylon lining to minimize the radioactive background eminating from the surrounding rock.

2.1 Neutrino Interactions

The unique sensitivity of the SNO detector actually lies in the neutral current (NC) reaction of the neutrinos with the deuterons:

$$\nu_x + d \rightarrow p + n + \nu_x \tag{2.1}$$

where ν_x represents the neutrino of all types. It is only through reaction (2.1) that the total neutrino flux can be determined. Detection of the neutral current events will be achieved by using a series ^{3}He proportional counters immersed in the heavy water. The downside of this interaction is that essentially all energy, directional, and some timing information are washed out from the thermalization of the neutron as it transverses through the heavy water [1].

Previous detection of $\bar{\nu_e}$ from SN1987A by Kamiokande II and IMB is due mainly to the charged current (CC) reaction:

$$\bar{\nu_e} + p \rightarrow n + e^+ \tag{2.2}$$

as light water consists mainly of protons. This reaction will still be observed by the SNO detector from the light water surrounding the acrylic vessel. Only a very few neutrinos will interact through electron scattering (ES) due to the small cross-section of this interaction:

$$\nu_x + e^- \rightarrow \nu_x + e^- \tag{2.3}$$

The neutrino to be detected through ES will be the ν_e since ES is mainly a charged current channel for ν_e . The charged current reactions for the deuteron will consist of ν_e and $\bar{\nu_e}$:

$$\nu_e + d \rightarrow p + p + e^- \tag{2.4}$$

$$\bar{\nu_e} + d \rightarrow n + n + e^+ \tag{2.5}$$

These reactions are particularly useful in extracting the energy of the neutrinos. The other more interesting aspect of the reactions (2.2) to (2.5) is the directional information on the source of the supernova. From the angular distribution of the events of those

[1]The thermalization length of neutrons in water is about 20 cm

Interaction	Detectable Particles	Q value
$\nu_x + e^- \rightarrow \nu_x + e^-$	e^-	0.0
$\bar{\nu_e} + p \rightarrow n + e^+$	e^+	1.44
$\nu_e + d \rightarrow p + p + e^-$	e^-	1.80
$\bar{\nu_e} + d \rightarrow n + n + e^+$	n, e^+	4.03
$\nu_x + d \rightarrow p + n + \nu_x$	n	2.22

Table 2.1: Summary of the available ν interactions of SNO detector that are important to supernova neutrino detection. The Q value is the threshold energy for the interaction to occur.

interactions, one could infer the position of the supernova in the sky. The accuracy with which this can be done is given by

$$\delta\theta \sim \frac{\Delta\theta}{\sqrt{N}} \tag{2.6}$$

where N is the number of detected electrons, and $\Delta\theta$ the angular resolution of the detector.

Chapter 3

Supernova Generator

Much efforts have been put in the modeling of Type II supernova since the detection of neutrinos from SN1987A. For every supernova model proposed, there will be a detector response prediction for all the existing or future neutrino detectors. Detector response for SNO to a generic Type II supernova has been calculated by Burrows and Klein [2].

The data analysis and simulation for SNO will be carried out using the SNO Monte Carlo Analysis software (SNOMAN). The software is designed with solar neutrino data analysis in mind. However, the software is still written to be as modular as possible to accommodate further development as described in this thesis. The overall architecture of SNOMAN is presented in the next section.

3.1 SNO Monte Carlo Analysis Software

SNOMAN is divided into a series of logical entities called Software Units (SUs). Each SU will perform certain well defined tasks. There are three types of SU in SNOMAN:

1. **Shell**. As the name implies, this is the outer framework of SNOMAN. Its main function is to call all processors and initialize any support they require.

2. **Processors**. These are the main engines of SNOMAN. The processors perform a set of operations on the data structure. One example of a processor is the Monte Carlo Event Generator whose main function to generate and simulate a set of events as seen by the detector. The user can independently switch on or off each processor according to his or her needs.

3. **Support Systems.** These provide the additional tools and information required by the processor to perform its task. Most support systems can be accessed by a wide range of processors but some are unique to a specific processor. An example of a support system would be the Geometry code which enables the Monte Carlo Event Generator to take into account the geometry of the detector in its calculation.

The software will first initialize itself by reading in commands from standard input. Additional commands stored in files can be included by instructing SNOMAN to read these files. These command (.cmd) files change the default processors and support systems to fit the needs of the user. They also contain basic input parameters like the energy of the electrons to be simulated. After initialization, SNOMAN will execute the processors called and output the results to a specific file. The output file formats available are the CERN Hbook format[1] or the SNO ZDAB unprocessed data format[2]. Further details on choosing the right output format, the different processors and support systems, and software database can be found in the SNOMAN user manual [4].

3.2 Motivation

As mentioned earlier, the generator codes written for SNOMAN have included the solar neutrino spectrum as part of their code. Presently, there is no support system in SNOMAN for other neutrino phenomena like atmospheric neutrinos and supernova neutrinos. The ability to simulate events for these two types of neutrino phenomena is crucial in the analysis of the neutrino data, especially as SNO goes online. The atmospheric neutrino problem will require more effort in determining the physics parameter before any useful simulation can be done. Supernova neutrinos, on the other hand, are quite well understood due to the work of Burrows, Janka and many others. The limiting factor for supernova neutrinos is the unpredictability of galactic supernova. The present estimates on the expected supernova rate go from one every 10 years to one every 100 years. Using the upper limit of one in 10 years, we might optimistically anticipate a galactic supernova

[1]The CERN Hbook format is a standard file format for writing Monte-Carlo analysis data to histogram which can be further manipulated by other softwares in the CERNLIB package

[2]ZDAB format is a file format that stores the unprocessed or raw data in particle physics. For SNO, it would contain the time and position of PMT hits

occuring before the end of the millenium.

By adopting the generic Type II supernova model of Burrows and Klein, a standard supernova generator code can be written for SNOMAN. The modularity of SNOMAN will ensure a trouble-free linking between the code and software. The generator code will be useful for the following reasons:

1. Ability to explore the sensitivity of the detector to extragalactic supernova (like SN1987A in the Large Magellanic Cloud).

2. Test the sensitivity of the detector to new physics parameters particularly neutrino mass.

3. Determine the angular resolution which is useful in tracing back the SN position in the sky. Since the neutrino signal is the first detectable signal for stellar collapse, this will provide an early warning system and a small sky search area for optical wavelength astronomers.

4. Determine the threshold on the number of events expected so that a proper SN trigger algorithm can be produced. This is also useful to test the response of the SNO electronics and the CPU designed for the SN Watch program.

3.3 SN Generator Code

In this section, the general concept of the SN generator code will be outlined and the exact procedure is presented in Chapter 4. The detected flux depends on the number of the neutrinos transversing the detector volume, which in turn, depends on the inverse square of the distance to the supernova. Therefore, the distance to the supernova will have to be a parameter in the generator code so that SN events at different distances can be simulated. A snag is encountered immediately: the inclusion of the distance as a parameter is completely new for SNOMAN (the Sun is never going to drift away from Earth). To overcome this problem, one would have to write a new processor code for SNOMAN and that would require an understanding of SNOMAN SUs. For the purpose of this work, it is decided to create a generator program which takes in the distance and outputs the other standard SNOMAN parameters (energy, time, etc) to a command file.

Interaction	Parameters
Neutral current	Position(D_2O); Time
Charged current	Position(D_2O, H_2O); Time; Energy; Angle
Electron scattering	Position(D_2O, H_2O); Time; Energy; Angle

Table 3.1: This gives a list of input parameters for the cmd file for each neutrino interaction. The position specifies whether the interaction occurs in the heavy water or the light water. The angular distribution would be able to point back the SN in the sky. The time for the first detected neutrino will be zero.

The standard database for this generator program would consist of the luminosity and energy of the neutrinos for a Type II supernova as calculated by Burrows *et al.* [1, 2]. Cross-section for the appropriate neutrino interactions with deuterons are obtained from the work by Nozawa [5] while for ES and proton interactions is based on [6]. With this information in place, one is able to produce the detected differential flux of the neutrino for the supernova. By sampling the detected differential flux, the distribution of the neutrinos' energy and arrival time can be obtained. These can then be converted to a command file output to simulate a series of events on SNOMAN. However, the neutrino energies first have to be converted to the electron, positron, or neutron energies since SNOMAN is unable to produce an interaction through a neutrino input. The energies of the resulting particles can be estimated by using relativistic kinematics calculation. Recalling Sec. 2.1, the neutron energy information will be lost due to the thermalization of neutron in the water, hence the parameters for neutron would be limited to the quantity, position, and time. Energy and direction inputs are needed for the CC and ES reactions which can then be used to calculate the angular distribution of the neutrinos. A summary of the required input parameters for each neutrino type is given in Table 3.1.

Another matter of concern is the statistics of the number of events observed by SNO. SNOMAN does not account for the primary neutrino statistics in any event generation. For any new class of neutrino phenomenon, the user has to ensure that the generator code includes the correct statistics for the number of events observed. Typical low rate supernova event obeys poisson statistics [7] while for a SN at 10 kpc, gaussian statistics

will be sufficient to describe the large number of events observed by the SNO detector. The generator will incorporate the choice of these statistics depending on the distance of the supernova.

Chapter 4

Signal Formalism

4.1 Neutrino Emission Model

The luminosities $\mathcal{L}(t)$ and energies $E_\nu(t)$ for each type of neutrino are based on the generic Type II supernova model of Burrows and Klein [1, 2]. From these two quantities, one can calculate the flux of the neutrinos arriving at Earth using

$$\mathcal{F}(t) = \frac{k}{4\pi R^2}\frac{\mathcal{L}(t)}{E_\nu(t)} \tag{4.1}$$

where R is the distance to the supernova in kilo-parsec [1], $k = 6.5545 \times 10^{17}$ (conversion factor to take care of the astrophysical units), $\mathcal{L}(t)$ is the luminosity of the neutrinos at time t of the supernova in 10^{51} ergs/s^2, and $E_\nu(t)$ is the energy of the neutrino produced from the supernova at time t in MeV. The observed differential neutrino flux at Earth will be a convolution of Eq. 4.1 and the neutrino spectrum as the neutrinos are emitted from the supernova. This is given by:

$$\frac{d^2N}{dE_\nu dt} = \mathcal{F}(t) f(\epsilon_\nu, t) \tag{4.2}$$

where the spectrum of the neutrino, $f(\epsilon_\nu, t)$ is found to be of Fermi-Dirac form [1]:

$$f(\epsilon_\nu, t) = \frac{\epsilon_\nu^2}{\exp^{\epsilon_\nu/T-\eta}+1}\left(\int_0^\infty \frac{\epsilon_\nu^2}{\exp^{\epsilon_\nu/T-\eta}+1}\, d\epsilon_\nu\right)^{-1} \tag{4.3}$$

where T is the temperature of the neutrino, ϵ_ν is the energy of the neutrino, and η is the degeneracy parameter. To obtain the detected flux for any detector, one needs to take

[1] 1 parsec (pc)= 3.26 light years. This is one of those weird units that astronomers used.
[2] 1 erg $= 1 \times 10^7$ joules.

into account the total number of target particles in the detector and the cross section of the interaction between the target particle and the neutrinos, giving:

$$\frac{d^2N_{det}}{dE_\nu dt} = N_T \sigma(\epsilon_\nu) \frac{d^2N}{dE_\nu dt} \tag{4.4}$$

where N_T is the total number of interacting particles and $\sigma(\epsilon_\nu)$ is the cross-section of the specific interaction.

The above analysis holds if one assumes a massless neutrino. For completeness, the mass of the neutrino will lead to a more generalized form of Eq. 4.4 as:

$$\frac{d^2N_{det}}{dE_\nu dt} = N_T \sigma(\epsilon_\nu) \frac{d^2N}{dE_\nu dt} \delta(t - t' - \Delta t) \tag{4.5}$$

where t is the detector time, t' is the time of emission, and Δt is the delay time for a relativistic massive neutrino. The delay time has the form:

$$\Delta t = \frac{R}{2c} (\frac{m_\nu}{\epsilon_\nu})^2 \tag{4.6}$$

The time delay will introduce a slight distortion in the time distribution of the observed spectrum. Small ν_e mass within the 4 to 10 eV range would be observable for a galactic supernova. SNO will definitely not be mute to a massive ν_τ, detectable through the NC interactions. Significant distortion of around 200 msec in the rise time would be observed for ν_τ of $\sim$ 10 eV mass. Maximal time delay of 300 msec on the ν_μ time distribution would be observed if the 17 KeV neutrino mass model proposed by Simpson [8] is true. Not only that, the proposed 17 KeV ν_τ will decay during its flight to Earth, resulting in a lower count rate for ν_μ . These minute distortions would be able to provide a direct measurement on the mass of the neutrino. It is thus crucial to have the precise measurement of each neutrino arrival time in order to gain insight to the neutrino mass problem. For the sake of simplicity, the generator code to be written will consider only massless neutrinos.

4.2 Sampling and Detection

One can calculate the required detected flux distribution for any interaction and neutrino type by substituting the appropriate cross-section $\sigma(\epsilon_\nu)$ into Eq. 4.4. This distribution

can then be sampled to get the neutrino energy distribution and the detected time distribution needed for the command files. The hit-and-miss rejection method is used to perform the sampling. Details of this method are presented in Appendix A. Special attention is paid to ensure the uniformity in the generation of the energy and time.

Once the energy distribution of the neutrino is output, the conversion to the resulting particles' energy is carried out. The neutrons from the neutrino interactions are assumed to be thermalized, requiring only their total number and time of creation to be written to the command file. The electrons and positrons resulting from NC and CC reactions will carry energies that are defined as the difference between the neutrino energy ϵ_ν and the threshold energy Q.

$$E_e = \epsilon_\nu - Q \tag{4.7}$$

The Q values for the different interactions are already summarised in Table 2.1. The energy for ES interaction is given by

$$E_{e^-} = \frac{2\epsilon_\nu^2}{(1 + 2\epsilon_\nu)} \tag{4.8}$$

derivable through relativistic kinematics. The region of interaction is specified either in the light water, heavy water, or both. The specific creation position in the medium is assumed to be isotropic.

The propagation direction of the electron is highly forward peaked, i.e., the electron will be scattered along the direction of the incoming neutrino. The exact angular distribution of ES is

$$\theta = \cos^{-1}\left[\sqrt{\frac{2E_{e^-}}{E_{e^-} + 2.0}}\left(\frac{1.0 + \epsilon_\nu}{\epsilon_\nu}\right)\right] \tag{4.9}$$

For the CC interaction, the angular distribution of the electrons or positrons is in the form of $1 - \frac{1}{3}\cos\theta$, giving a 7:5 backward-forward asymmetry. The only advantage of this interaction is the large number of events through this channel. These angular distributions have to be converted to the direction cosines with respect to the center of the detector. This procedure is required as part of SNOMAN's inputs. The output form of the direction cosine distribution will still preserve the 7:5 asymmetry. Once the diection cosine of the incoming neutrino is input, a subroutine called *Rayleigh Scattering*[3] will

[3]This code is part of the standard SNOMAN routines.

automatically determine the direction cosine distribution of the outgoing photons caused by the electrons or positrons shower. By fitting the direction cosine distribution of the resulting particles, one could obtain the position of the supernova in the equatorial coordinate system through a non-trivial transformation outlined in Appendix B. Ultimately, the ability to pinpoint the supernova position depends on the total number of events observed.

Chapter 5

Results

In this chapter, the results obtained using the supernova generator code are presented. Comparisons are made between the results of this thesis and those of Burrows [3] and the SNO Proposal [9], both of which give a very effective diagnostic tool for code-correction.

5.1 Event Distribution

By sampling the normalized detected neutrino flux, $\frac{d^2N_{det}}{dE_\nu dt}$, the event distribution for each species of neutrinos can be obtained. This event distribution will contain information on the expected number of events observed for a certain energy and time. Essentially, the event distribution represents the detector response to the supernova. A sample of the event distributions for a 10 kpc SN as seen by SNO is shown in Fig. 5.1. Total recorded events for ν_e is 130, while $\bar{\nu}_e$ and ν_μ have 450 and 210 events respectively.

The many orders of magnitude over which the time data are collected from a supernova pose a problem in the time sampling. Many details are contained within the first 500 msec while events will continue to be observed over the next 40 sec, during the cooling phase. The huge spike during the first second represents events from the burst phase and the explosion phase. The large time bin used in the distribution completely washes out the finer details of the distribution. A more insightful way of extracting information from the event distributions is to perform stand-alone binning of the time and energy. The time binning is presented in Sec. 5.1.1. A rough estimate using the event distributions indicated that the number of neutrinos detected before the explosion will be about the same as the number detected during the cooling phase.

From the distributions shown in Fig. 5.1, ν_e events tend to be lower in energy while $\bar{\nu}_e$

will have intermediate energy and ν_μ will have the highest energy. The energy order for the different neutrinos is due to the neutrino opacity within the core. Neutrino opacity arises mainly from the neutrino scattering with nuclei or free nucleons in the core. For a protoneutron star, the neutron-rich outer core will make the $\bar{\nu_e}$ opacity smaller than ν_e opacity since the charged current interaction of ν_e with the free neutrons has a large cross-section. The smaller opacity of $\bar{\nu_e}$ will allow us to see deep into the core to higher temperatures $\bar{\nu_e}$. Since ν_μ only participate in neutral current interactions (with small cross-section), the energy of ν_μ is the highest. Binning the energies will yield the energy distribution of the neutrinos which is presented in Sec. 5.1.3.

5.1.1 Count Rate

The count rate computed will give an early indication on the number of expected events seen by a detector. The count rate is derived by summing the fluxes over all the energies for a given time. The computed count rate using Burrows' model is shown in Fig. 5.2. The count rate shown is actually the time distribution for each of the neutrinos. Here, the details during the first second are shown clearly, unlike that of the event distribution graph.

Refering to the figure, the count rate for the ν_e is exceedingly high during the first few milliseconds, a direct consequence of the shock breakout. Within 20 msec, the count rate of ν_e decreases rapidly and stabilizes around 200 counts per second. The small cross-section and low energy of ν_e will push its count rate below that of $\bar{\nu_e}$ and ν_μ . The ν_e signal will be the dominant signal early on, marking the birth of the supernova. The signal from ν_μ lies between that of ν_e and $\bar{\nu_e}$. Due to its high energy (i.e., higher cross-section), ν_μ will interact with the deuteron to give an appreciable number of events. From the figure, the dominating signal seems to come from $\bar{\nu_e}$. Despite the lower luminosity, $\bar{\nu_e}$ has the most interacting targets in SNO: the proton in the light water, the deuteron in the heavy water and the electrons in the water. Not only that, the cross-section of $\bar{\nu_e}$ on protons is the highest among all the interactions. In fact, the event contribution from the light water with $\bar{\nu_e}$ alone is comparable to that of the heavy water for the other two species of neutrino.

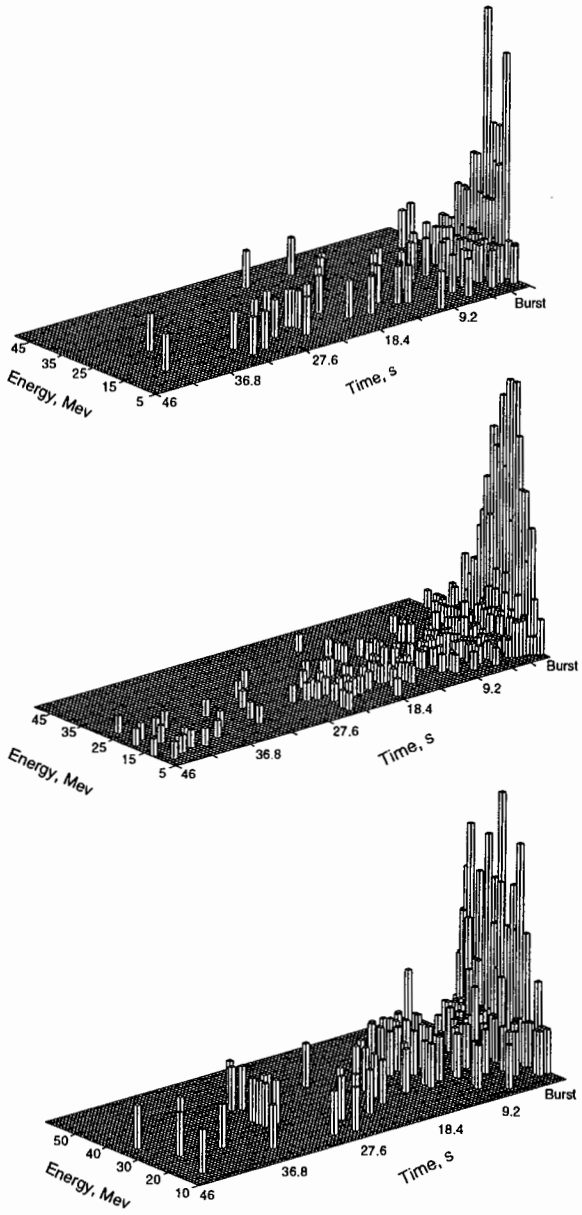

Figure 5.1: Event distribution for ν_e , $\bar{\nu_e}$, and ν_μ (from top to bottom). The number of events for the neutrinos in the same order are 130, 450 and 210. A single event on the plots is a lone single colume at later time in the histogram.

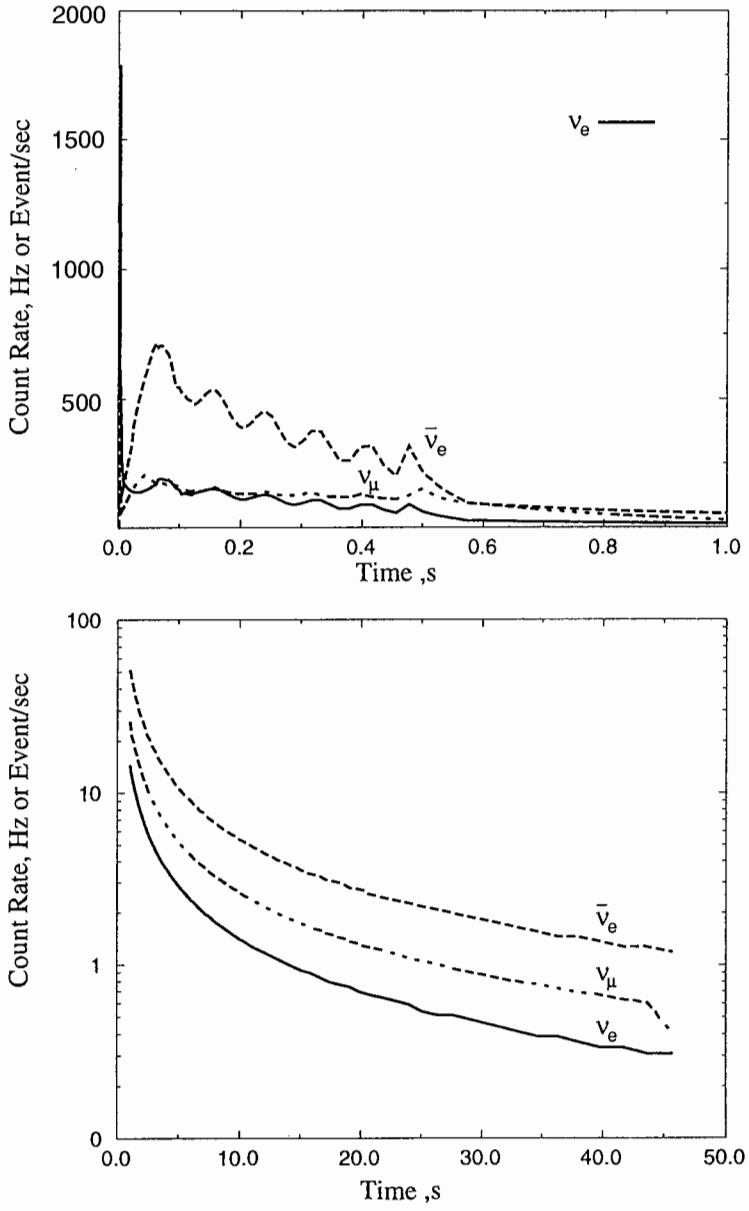

Figure 5.2: Count rate of SNO for a 10 kpc SN. Both heavy water and light water events are included. $\bar{\nu_e}$ has the highest count rate followed by ν_μ and ν_e .

5.1.2 Expected Events

Knowing the number of expected events will automatically place a detection limit on the distance of the supernova. The number of events observed will have direct implications on the physics of the supernova itself. Another reason for placing such emphasis on the number of expected events is the high statistics required to study the mechanism of the supernova.

The integration of the count rate over the period of emission will yield the total expected rate for the supernova. By integrating over certain areas of interest, like burst and cooling, one can obtain the expected events for this time interval. These expected rates are computed and compared with the works mentioned earlier. The results are summarized in Table 5.1. The error for this work is mainly from the inaccuracy in the neutrino luminosity values and the error introduced in the calculation of cross-section for Fig. 5.2. The burst time is defined to be from the time $t = 0$ s to $t = 10$ ms as stated in the original 1987 SNO Proposal; the remaining time is the cooling time. Clearly there is a discrepancy between the number of events from the SNO Proposal and the work presented in this thesis. Burrows' work only publishes the total number of events expected for each reaction. Those numbers are compared with this work and found to agree within the calculation error of 3%. Discrepancy between the Proposal and this work is hardly a surprise since the SNO Proposal assumed the supernova model of Bowers and Wilson [10], which predates SN1987A and has been superseded by the more accurate work of Burrows.

5.1.3 Energy Distribution

Binning the energy from the event distribution produces the energy distribution for the detected neutrino. The distributions are shown in Fig. 5.3 from which one can see that the neutrino energies are clustered around the 20 – 30 MeV range. The average energies for the detected neutrinos are 16.5 ± 1.5 MeV for ν_e , 18.2 ± 0.9 MeV for $\bar{\nu_e}$, and 26.0 ± 1.8 MeV for ν_μ . The errors quoted are assumed to be 1σ gaussian error. A clear deficit of high energy neutrinos are present while in some cases, the lower energy neutrinos are absent. The lack of low energy neutrinos can be attributed to the threshold

Reaction	Burst		Cooling		Total Events		
	SNO	Thesis	SNO	Thesis	SNO	Thesis	Burrows
$\nu_x + d \rightarrow p + n + \nu_x$	6	4	760	273	766	277	272
$\nu_x + e^- \rightarrow \nu_x + e^-$	1	1	16	20	17	20	22
$\nu_e + d \rightarrow p + p + e^-$	10	6	33	77	43	83	82
$\bar{\nu}_e + d \rightarrow n + n + e^+$	0	0	20	68	20	68	67
$\bar{\nu}_e + p \rightarrow n + e^+$	0	0	120	335	120	335	331

Table 5.1: A comparison between the SNO Proposal, Burrows, and the generator code. The generator code adopted the Burrows' model, hence the number of events agree with Burrows'. SNO proposal uses Bowers-Wilson model which give a different number.

of the detector whereas the deficit of high energy neutrinos is attributed to the Fermi-Dirac spectra cutoff for these neutrinos. The distribution can be fitted almost perfectly with a thermal Maxwell-Boltzmann distribution. However, the fit fails to account for the higher energy neutrinos. This is due to the distortion in the energy spectrum by the cross-section of the interactions. Most of the interactions have higher cross-sections at higher energies, making interaction possible, thus leading to the tailed distribution in the energy spectrum. The shape of the energy distribution may provide clues on the nucleosynthesis process within the supernova [11].

5.2 SNOMAN's Output

With a correct time, energy and direction distribution, SNOMAN is able to simulate detector response for the supernova neutrinos. These distributions were linked into the SNOMAN user-routine and the final test entails the reproducibility of these distributions.

The energy distribution linked into SNOMAN is of a thermal distribution form, as described in Sec. 5.1.3. Linking is achieved by specifying the appropriate energy distribution for any interaction in the file *en_user.for*. One is able to specify a user distribution in a .cmd file to allow sampling by SNOMAN. A comparison between the output distribution of SNOMAN and the original distribution for reaction 2.2 is shown in Fig. 5.4.

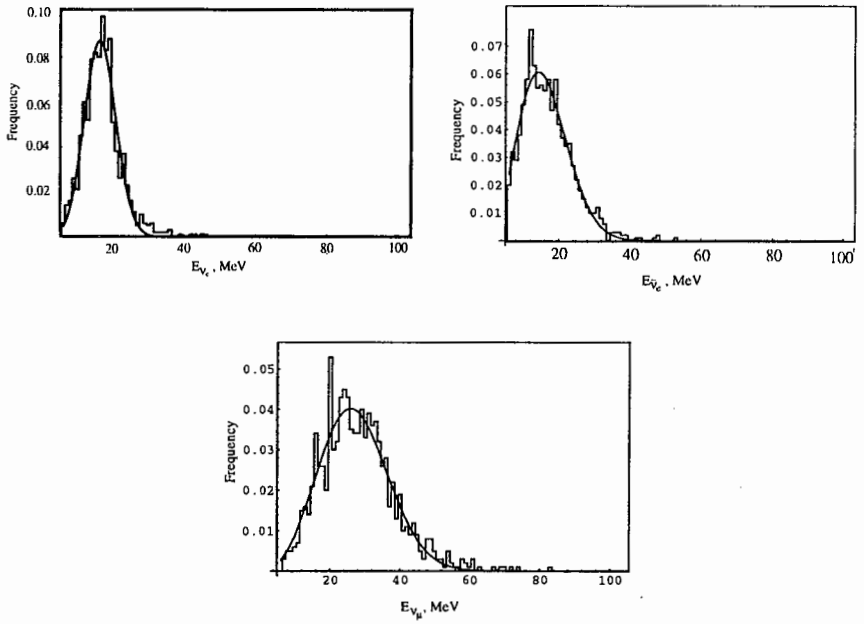

Figure 5.3: Energy distribution for ν_e , $\bar{\nu}_e$, and ν_μ . The distribution is for 1000 samples from the normalized detected neutrino flux distribution and normalized to unity area. The fit shown is of a thermal distribution. Notice the tail does not fit well.

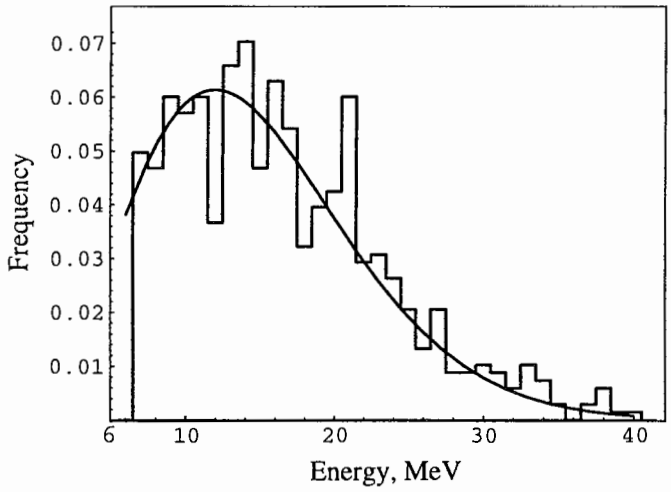

Figure 5.4: Comparison between the generator's sampled energy distribution and that output by SNOMAN. SNOMAN is able to sample and output the distribution correctly. The fit is that from the generator.

It is clear that the linking is successful since SNOMAN is able to reproduce the same distribution. The only shortcoming in this sampling is that not all events are simulated successfully due to the inefficiency of the event fitter. The event fitter has an effficiency of around 80%

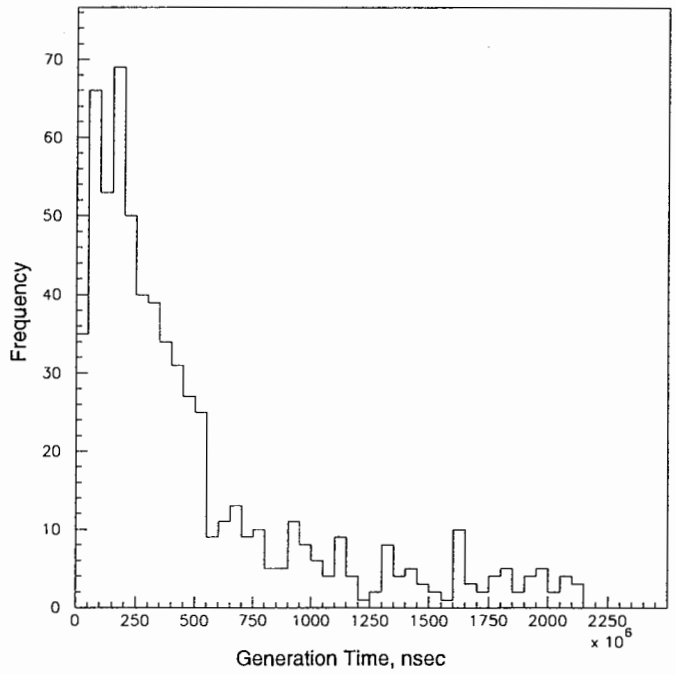

Figure 5.5: Time distribution output by SNOMAN. These times are not reasonable because of the difficulty in extracting time from SNOMAN.

A similar exercise is performed on the time distribution through the calling of the file *time_user.for*[1] in the .cmd file. The SNOMAN output is shown in Fig. 5.5. It may seem that SNOMAN is unable to reproduce the time distribution as requested. Closer examination using the standard SNOMAN feature has indicated a possible problem within the time storage bank. Generating duo events 20 sec apart using the standard feature produces negative generation time in the Hbook file. Since time is stored in nanoseconds within SNOMAN, the long time elapse of the events may cause a memory overflow with the time storage bank. Attempts to correct this problem using the other available time

[1]It should be clear that the user routine is given the suffix *_user* in SNOMAN.

storage banks also lead to the same problem. This problem has to be addressed if one is doing supernova analysis since the time distribution is absolutely critical in determining mass of the neutrinos. Fortunately, this problem will not affect the Monte-Carlo event generation in SNOMAN since the storage bank and the generator bank are two different routines.

The direction distribution of the events is called from *dir_user.for*. For an arbitrary choice of neutrino direction, the distribution of the direction cosines gets washed out by the scattering. A more obvious choice of (0,0,1), where the supernova is directly over the zenith of the detector, is used for the direction cosines. The direction cosines distribution obtained for a 643 event simulation of reaction (2.2) are shown in Figure 5.6. Since the direction cosines for x and y are at zero, they are expected to be uniformly distributed for the whole range of angles, as shown in Figure 5.6. For the z components, one could see a clear backward-forward asymmetry. Through Ntuple manipulation, the number of backward events is 383 while the forward is 260, giving a ratio of 1.47 ± 0.18, assuming $\sqrt{N}$ error, which is in agreement with the 1.4 ratio.

As for the ES interaction, the angular distribution is highly forward peaked, which is illustrated in Fig. 5.7. No plots for x and y are shown for ES since the direction cosines for the two axes have a peak at zero. These ES events are the actual simulation of a 10 kpc SN. From Fig. 5.7, the ES events will only be able to point us back to the supernova to within $15° \pm 3°$. Such angular resolution is considered a nightmare for astronomers who have to search at least 100 million galactic stars in that sky coverage. Using the CC events, the angular resolution is decreased down to $4.0° \pm 0.7°$. This is a significant improvement, but still inadequate for the astronomers. Undoubtedly, the best angular resolution will be coming from SuperKamiokande due to its large volume and the many ES events available.

5.3 Simulation of SN1987A

A mock simulation of SN1987A is performed using the generator. The total number of events that would have been observed by SNO is found to be 33 ± 6 events. Out of these, 5 were from ν_e , 20 from $\bar{\nu_e}$, and 8 from ν_μ . These events are summarized in the event

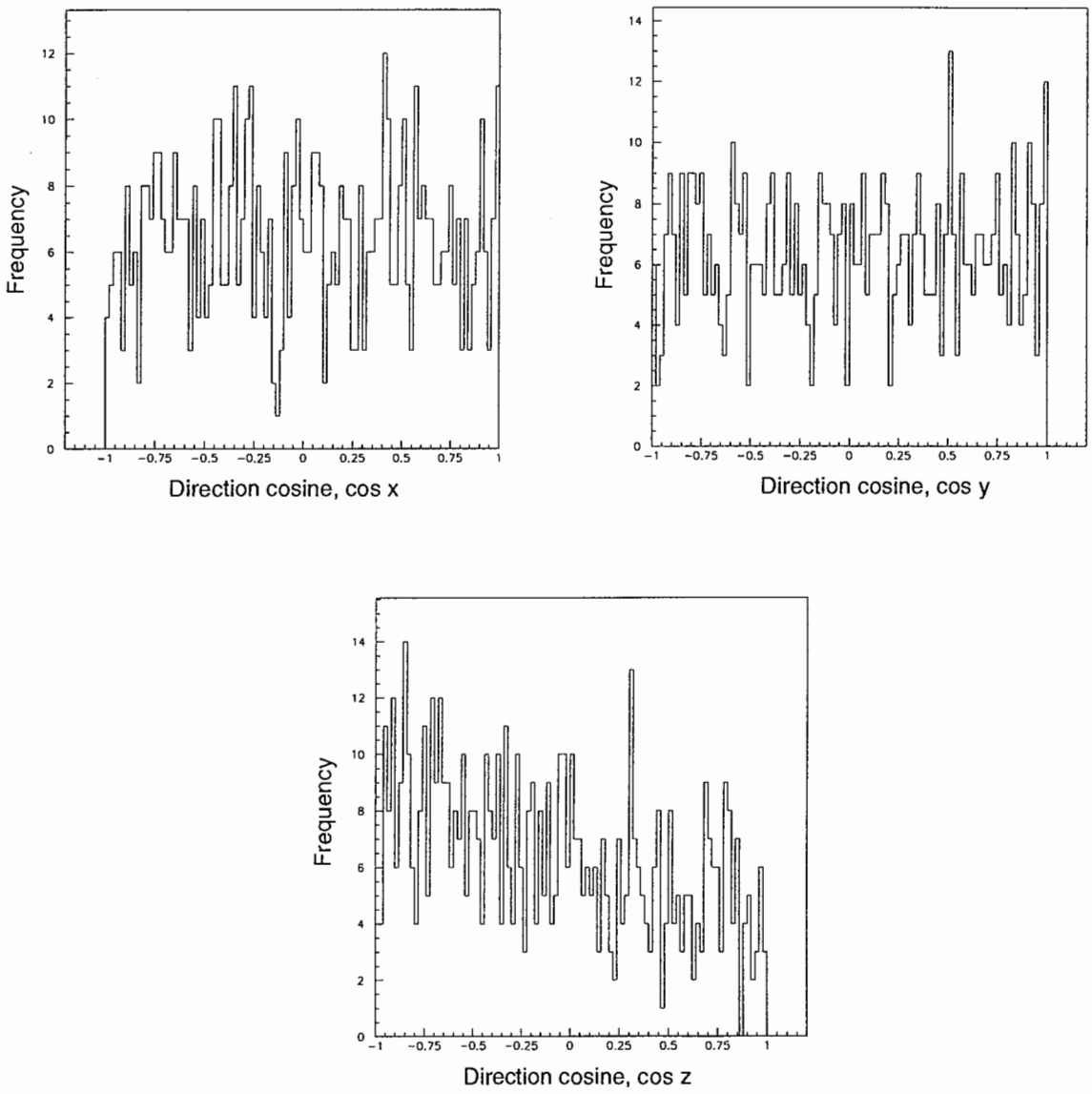

Figure 5.6: SNOMAN's fitted direction cosine distribution for $\bar{\nu}_e + p$. The direction cosines for x and y are pretty much constant. However, the direction cosines for z has the 7:5 backward to forward asymmetry. The total number of events is 643.

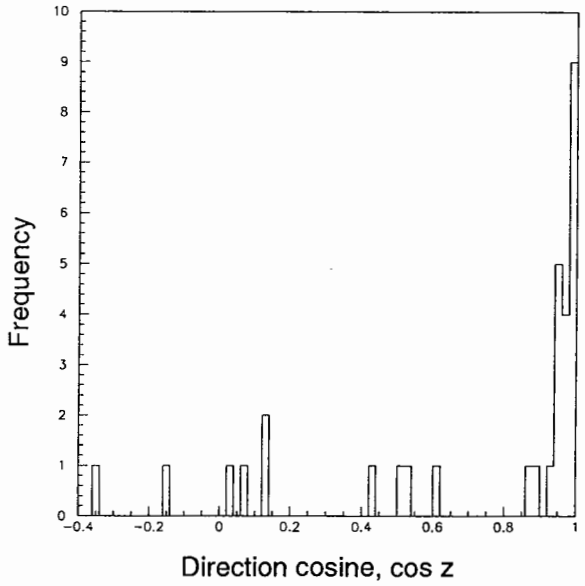

Figure 5.7: SNOMAN fitted direction cosine for 31 ES events. The direction cosine is clearly forward peaked at $\cos z = 1$.

distribution plot in Fig. 5.8. Some of the events may be lost in the background due to their lower energies and the time elapsed between the events. Estimating from the efficiency of the event fitter in SNOMAN, we may only be able to account for about 28 of the events.

Some comparisons can be made with the observed data by IMB and Kamiokande. Considering only the $\bar{\nu}_e$ events, the average energy of the neutrinos is 19.4 ± 4.3 MeV while the energy from IMB and Kamiokande gives 21.6 ± 4.7 MeV. The error for this simulation is assumed to be a Poisson error. It is somewhat difficult to compare the energy and time distributions since the number of neutrinos detected are so few. Generally, the range in energies seen by SNO is almost identical to that of Kamiokande (see Fig 5.9. There are not as many high energy events occuring in the simulation than what is yielded by IMB. Again, there is nothing astounding with this slight discrepancy since the SNO "data" are only one of the many samples available. It should be noted too that the energy threshold for IMB detector is 30 MeV, so its sensitivity lies mainly in the high energy regime.

SNO is not much better than Kamiokande and IMB in determining the location of

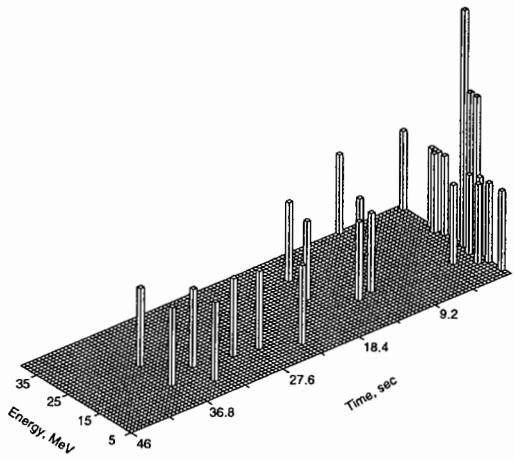

Figure 5.8: Event distribution of SNO for a 50 kpc SN. All neutrinos are included in the plot. Total number of events is 33.

SN1987A. The dominant events are through the CC channel (20 CC events) while the rest are NC events. Virtually no ES events are obtained. Working with the 20 CC events will only provide a resolution of comparable to that of Kamiokande.

5.4 Future Implementations

The generator code is, by far, a completed work. Some of the features that can be added into the next version[2] of the code are listed below:

1. A supernova model code that can generate the luminosity and energy of the neutrino accurately. This can be obtained probably through collaborating with Burrows.

2. Inclusion of the neutrino mass as a parameter. The time spectral distortion mentioned in previous section can then be simulated.

3. Proper linking with SNOMAN via the SNOMAN's processor route. A difficult task for a novice SNOMAN user, otherwise an achievable task for the many SNOMAN authors.

[2]A favorite term among commercial software writer but frustrates the end user.

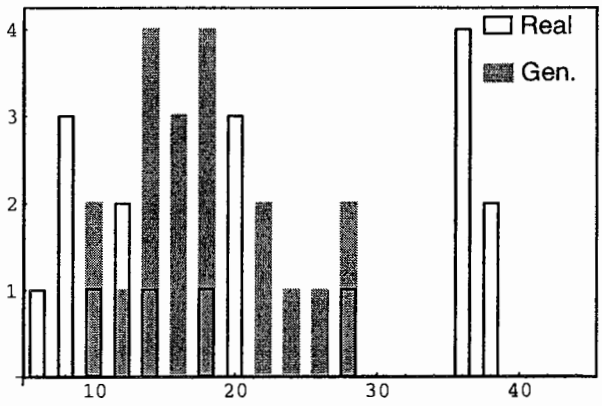

Figure 5.9: Energy distribution comparison between observed and simulated $\bar{\nu}_e$ events for a 50 kpc SN. Observed data are taken from IMB and Kamiokande. Total number of events for both cases is 20.

Chapter 6

Conclusions

By adopting the generic Type II supernova model of Burrows and Klein, a supernova generator code is has been written for the SNO analysis software, SNOMAN. To test the validity of the code, results produced by the code are compared with the published results of Burrows and the SNO proposal. In all cases, the generator code is able to reproduce the results of Burrows. A discrepancy in the expected number of events is found between the original 1987 SNO proposal and the work of this thesis. This may be attributed to the different supernova model used in the calculations. The average energies of the neutrinos detected by SNO are 16.5 ± 1.5 MeV for ν_e , 18.2 ± 0.9 MeV for $\bar{\nu}_e$, and 26.0 ± 1.8 MeV for ν_μ . The number of events observed prior to the supernova explosion will be approximately the same as the cooling phase.

SNOMAN now is able to output the supernova's energy and direction distribution. However, due to a problem with SNOMAN's time storage bank, SNOMAN is unable to output the correct time distribution. This problem has to be fixed by the SNOMAN authors. Simulations of ES and CC events for a 10 kpc SN using SNOMAN yield a theoretical directional resolution of $4.0° \pm 0.7°$ for the SNO detector. Such a resolution is inadequate for the astronomers to locate the supernova. This is an expected limitation for a small volume neutrino detector like SNO.

As a final test on the generator, a 50 kpc SN (same distance as SN1987A) simulation is performed. Better comparisons with observations can be made by considering the $\bar{\nu}_e$ events only. The average $\bar{\nu}_e$ energy obtained by the generator is 19.4 ± 4.3 MeV while the average energy detected by IMB and Kamiokande combined gives 21.6 ± 4.7 MeV. The total number of events of $\bar{\nu}_e$ expected for SNO is 20. This number is equal to the combined number of events observed by IMB and Kamiokande. The directional resolution

of SNO is not much better than the other two detectors due to the few numbers of events. Overall, the supernova generator code has demonstrated its ability to generate supernova neutrinos that conformed to the predicted signal of Burrows and also able to link with the analysis software.

Appendix A

Rejection Method

The outline of the rejection method is as follows: For a probability function in two dimensions[1], $p(x)$, that one wishes to generate, a comparison function $f(x)$ is used to enclose $p(x)$ for testing. A random deviate x_i is first generated with the corresponding test value R_i drawn within the comparison function (see Fig. A.1). If R_i is less than the value of $p(x_i)$, then x_i will be accepted or rejected otherwise. The cycle is repeated until the desired number of random numbers is generated. This method is easily implemented for a higher dimension distribution though not very efficient at times. If the distribution encountered is quite narrow, then the rejection method is highly inefficient. From the figure, choosing a comparison function that follows the probability function closely will reduce the test area and improve the efficiency.

The random number generator, ran3, from Numerical Recipes [12] is used in the sampling code. The comparison functions tried are the unit square function and a sequence of step functions. No appreciable improvement in speed is noted. The inefficiency in the first comparison function is offset by the small number of points to be generated (1000 points takes about two minutes on a Pentium 100 for both cases).

[1]This argument can be extended to higher dimensions

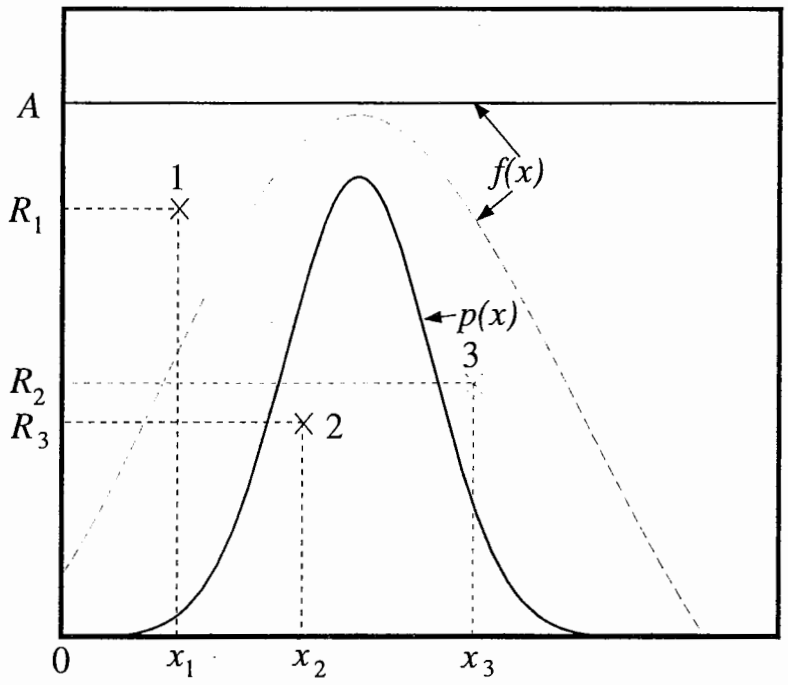

Figure A.1: Rejection method used for sampling the distribution $p(x)$. Two possible comparison function are shown, a line or a curve that encloses the distibution function. The values of $p(x)$ for the random deviates x_1, x_2, x_3 are compared with the corresponding test values R_1, R_2, R_3 taken from the comparison function. Value that lies within the area of $p(x)$ is accepted. In this case, x_2 will be accepted since R_2 is is within the area. x_1 would have failed the test with the line as a comparison function while x_3 would have failed for both test functions. Noticed that the efficiency of the curved test function is greater than the line since the area covered is less.

Appendix B

Coordinate Transformation

The standard coordinate system to represent position in the celestial sphere is the equatorial coordinate system. In this system, the position of any celestial object is specified by three parameters: the right ascension (RA or α), the declination (Decl or ϕ), and the hour angle from the constellation Aries (H or τ). The reader will have to refer to an introductory Astronomy textbook for the definition of each term.

By defining the general hour angle h as:

$$h = \tau - \alpha \tag{B.1}$$

the transformation between the local horizon coordinate system and the equatorial coordinate system is given by this set of equations:

$$\cos\psi = \sin\varphi\sin\phi + \cos\varphi\cos\phi\cos h \tag{B.2}$$

$$\sin\psi\sin z = -\cos\phi\sin h \tag{B.3}$$

where z and ψ are the azimuth and latitude in the horizon system respectively, with $\varphi = 46.5°$ being the latitude of Sudbury. Converting to the direction cosine with respect to the center of the detector requires the following equations:

$$\cos x = (1.0)/l \tag{B.4}$$

$$\cos y = (\tan\psi)/l \tag{B.5}$$

$$\cos z = \left(\tan z\sqrt{1+(\tan\psi)^2}\right)/l \tag{B.6}$$

$$l = \sqrt{(\cos x)^2 + (\cos y)^2 + (\cos z)^2} \tag{B.7}$$

where l is the normalization factor. Notice that transformation equations are invalid whenever the source lies on the any of the axes. If such a scenerio occurs, the code written is still able to output the right direction cosines by considering each axis separately. The formulation of the direction cosines may best be understood by refering to Fig. B.1.

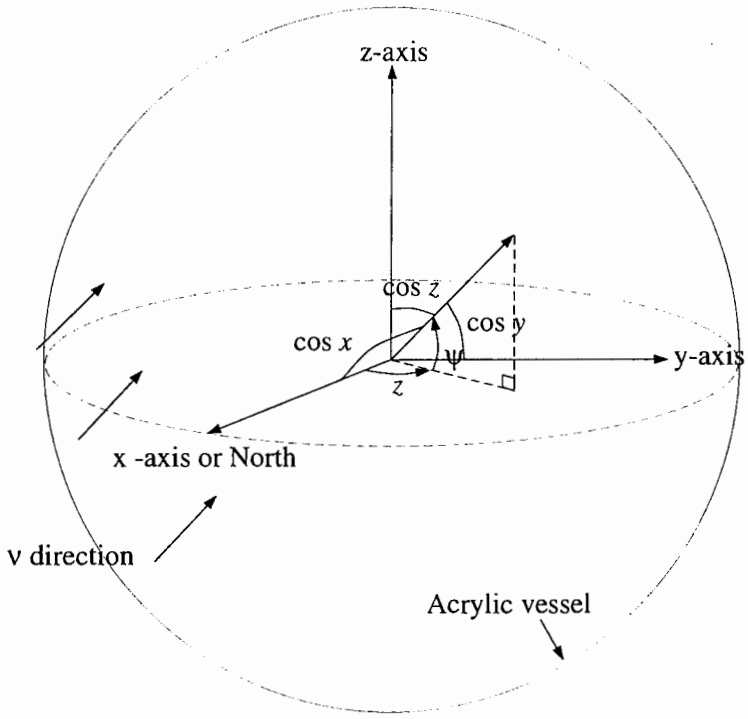

Figure B.1: Diagram for the derivation of the direction cosines from the local horizon system. The center of the detector is assumed to be the origin. the x-axis correspond to North. The projection onto the x-axis is assumed to be one.

Bibliography

[1] A. Burrows and E. Myra, *Ap. J.* **364** 222 (1990).

[2] A. Burrows, D. Klein, and R. Gandhi, *Phys. Rev. D* **45** 3361 (1992).

[3] A. Burrows, *Annu. Rev. Nucl. Part. Sci.* **40** 181 (1990).

[4] *SNOMAN User's Manual v3.00, Unpublished* (1996).

[5] K. Kubodera and S. Nozawa, *Int. J. Mod. Phys.* **E3** 101 (1994).

[6] J. Aratune and M. Fukugita, *Phys. Rev. Lett.* **59** 367 (1987).

[7] T. Loredo and D. Lamb, in *Fourteenth Texas Symposium on Relativistic Astrophysics*, edited by E. Fenyes (Academic Sciences, New York, 1989), p. 601.

[8] J.J. Simpson, *Phys. Rev. Lett.* **54** 1891 (1985).

[9] G. Ewans *et al. SNO Proposal* SNO-87-12 (1987).

[10] R. Bowers and J.R. Wilson, *Ap. J.* **263** 366, (1982).

[11] R.L Epstein, S.A. Colgate, and W.C. Haxton, *Phys. Rev. Letters* **61** 2038, (1988).

[12] W.H. Press, S.A. Teukolsky, W.T. Vettering, B. Flannery, *Numerical Recipes in C* (Cambridge University Press, 1992), p. 283.